On the precision and accuracy of structural analysis of light-induced metastable states

Vincent Legrand, Sébastien Pillet, Hans-Peter Weber, Mohamed Souhassou, Jean-François Létard, Philippe Guionneau, Claude Lecomte

On the precision and accuracy of structural analysis of light-induced metastable states

Vincent Legrand,[a,b] Sébastien Pillet,[a]* Hans-Peter Weber,[c] Mohamed Souhassou,[a] Jean-François Létard,[d] Philippe Guionneau[d] and Claude Lecomte[a]

[a]Laboratoire de Cristallographie et Modélisation des Matériaux Minéraux et Biologiques, UMR CNRS 7036, Nancy-Université, BP 239, 54506 Vandoeuvre-les-Nancy, France, [b]Institut Laue Langevin, 6 rue Jules Horowitz, BP 156, 38042 Grenoble Cedex 9, France, [c]ACCE, Grand Vivier, F-38960 St Aupre, France, and [d]Institut de Chimie de la Matière Condensée de Bordeaux, ICMCB CNRS, Université Bordeaux 1, 87 avenue du Docteur Schweitzer, 33608 Pessac Cedex, France. Correspondence e-mail: sebastien.pillet@lcm3b.uhp-nancy.fr

Bragg diffraction data were collected on single crystals of the spin-crossover complex $[Fe(phen)_2(NCS)_2]$ in its low-spin and light-induced metastable high-spin states. Experimental variables included the temperature (32 and 15 K), the X-ray source (sealed tube and synchrotron), and the time interval between laser light excitation of the sample (λ = 647 nm). From a comparison of the structural parameters refined, it is shown that photo-crystallographic measurements suffer significantly and systematically from bias if the probed sample contains residual ground-state species, resulting from an incomplete photo-conversion or a significant metastable- to ground-state relaxation. It follows that a 4% population of species in a different spin state affects the Fe—N bond lengths by more than three standard deviations, and the FeN_6 polyhedron volume by as much as seven standard deviations, while the mean atomic position misfit exceeds 0.005 Å.

1. Introduction

Single-crystal X-ray diffraction is a particularly well established technique in condensed matter physics that has enabled the study of many structure–property correlations, especially in molecular solids. In the past, such studies have been restricted to equilibrium ground-state systems; this limit has been overcome and extended to non-ambient conditions. Diffraction measurements under external perturbation such as pressure (Katrusiak & McMillan, 2004), electric field (Hansen *et al.*, 2004) or optical excitation (Coppens *et al.*, 2005; Cole, 2004), commonly termed steady-state perturbation diffractometry, are being explored increasingly. Diffraction data from samples under pressure are now widely collected, even though difficulties inherent to high pressure have to be overcome (*e.g.* the restricted angular opening of pressure cells limits the resolution available). Many solid-state processes can be triggered or driven by optical photon absorption. Depending on the reversibility and time scale of the solid-state physical phenomenon investigated (ms, ns, ps), several photo-crystallographic experimental setups have been designed specifically for laboratory (White *et al.*, 1994) and synchrotron X-ray sources (Coppens, 1992; Wulff *et al.*, 1997; Fullagar *et al.*, 2000). For very long-lived species (lifetime greater than hours), a conventional laboratory setup suffices. All of these take advantage of the fast data collection opportunities afforded by CCD area detectors. These experimental techniques are now being applied to the characterization of structural relaxation processes (Techert & Zachariasse, 2004), long-lived metastable states (Coppens *et al.*, 2002), short-lived excited states (Collet *et al.*, 2003; Coppens *et al.*, 2005) and solid-state photo-chemical reactions (Ohba & Ito, 2003; Friscic & MacGillivray, 2005). In parallel, specific structural refinement procedures (Ozawa *et al.*, 1998) and raw data analysis through singular value decomposition methods (Rajagopal *et al.*, 2004) have been developed. Experimental guidelines for time-resolved powder and single-crystal X-ray diffraction techniques applied to light-induced phenomena have been given (Davaasambuu *et al.*, 2004; Cole, 2004). Recently, one of us (Legrand, 2005) reported on the electron density analysis of the light-induced metastable state of $[Fe(phen)_2(NCS)_2]$, and this has encouraged us to pursue the development of the technique used in this work.

The goal of the present study is to address the question of precision and accuracy of the structural parameters derived for metastable states from steady-state perturbative single-crystal X-ray diffraction methods. Light excitation is considered here, but the conclusions may be extended to other perturbation means. The usual experimental procedure consists of shining light from a lamp or a laser onto a single crystal; the exposure is timed empirically to reach a photo-stationary state, at which point diffraction data are collected as quickly and accurately as possible. To this end, the use of a CCD area detector is almost mandatory. The crystal structure

of the metastable state is then derived using standard least-squares refinement software, as for a conventional crystal structure determination. The choice of suitable excitation conditions in terms of wavelength, bandwidth (broadband or monochromatic), power, and duration is a prerequisite to any accurate photo-crystallographic measurement. This is generally accepted. However, subtle hidden effects can affect the measurements and bias the results. These biases have never been thoroughly investigated, let alone described in the literature. The systematic errors introduced by badly chosen experimental conditions need to be quantified definitively. In some experiments, light excitation of the sample is carried out prior to the data collection (Ichiyanagi *et al.*, 2006; Niel *et al.*, 2005; Marchivie *et al.*, 2002; Money *et al.*, 2003; Thompson *et al.*, 2004; Huby *et al.*, 2004; Legrand, 2005), while in others the sample is irradiated continuously during the data collection (MacLean *et al.*, 2003; Kusz *et al.*, 2005). The choice of excitation conditions is important as it affects the precision and accuracy of the derived crystal structure. In the case of an incomplete ground-state to metastable-state photo-conversion, the probed single-crystal contains both species, with an unknown spatial distribution. The analysis of this effect is similar to that of treating static disorder in a usual structural refinement. In the case of an incomplete photo-conversion (see *e.g.* Kovalevsky *et al.*, 2005; Turowska-Tyrk, 2003; Enkelmann *et al.*, 1993; Bowes *et al.*, 2006), one commonly models both species, including the ratio of metastable- to ground-state species in the form of a molecular occupancy factor. However, the errors in the structural parameters due to such residual ground-state species have never been quantified. In the following, we wish to draw attention to the many difficulties inherent to such structural refinements, of which several crucial parameters are: (i) the structural contrast between the ground and the metastable state, (ii) the lifetime and relaxation kinetics of the metastable state, (iii) the excitation conditions, such as power and wavelength of the light source, measurement temperature, excitation duration and continuous or pulsed excitation. We wish to study the influence of these parameters for a real case. For this purpose, we chose the spin-crossover complex $[Fe(phen)_2(NCS)_2]$ as a representative system, since its ground-state and light-induced metastable-state properties have been widely investigated and the corresponding crystal structure reported (Marchivie *et al.*, 2002).

$[Fe(phen)_2(NCS)_2]$ is a spin-crossover coordination complex characterized at the molecular level by a high-spin (HS, $S = 2$) $\leftrightarrow$ low-spin (LS, $S = 0$) equilibrium (Gütlich *et al.*, 1994; Gütlich & Goodwin, 2004). The conversion from LS state at low temperature to HS state at higher temperature is driven by an entropy increase related to a change in the Fe—N bond length. At very low temperature, as demonstrated by Decurtins *et al.* (1984), spin-crossover complexes may also exhibit a light-induced excited spin-state trapping (LIESST) phenomenon. In this process, optical pumping takes place from a thermodynamically stable LS state to an often complete population of the quintet HS state. Relaxation to the ground LS state occurs at very low temperature through a multiphonon non-adiabatic tunnel process, and at higher temperature by means of a thermally activated process. The relaxation rate is therefore temperature-dependent, especially in the thermally activated region. The crystal structures of several spin-crossover materials in the metastable HS-2 state have already been described (Ichiyanagi *et al.*, 2006; Niel *et al.*, 2005; Marchivie *et al.*, 2002; Money *et al.*, 2003; Thompson *et al.*, 2004; Huby *et al.*, 2004; Legrand 2005; MacLean *et al.*, 2003; Kusz *et al.*, 2005). Magnetic and Mössbauer measurements show that our present test compound, $[Fe(phen)_2(NCS)_2]$, undergoes a very abrupt first-order thermal spin transition, centred at $T = 176$ K (König & Madeja, 1967). The crystal structure was analyzed in the *Pbcn* space group for both HS state (293 K) and LS state (130 K). Although it does not reveal any crystal symmetry change during the thermal transition (Gallois *et al.*, 1990), typical structural modifications are nevertheless observed at the transition: a shortening of the Fe—N(phen) and Fe—N(CS) bond distances (by 0.20 Å and 0.10 Å, respectively) and a more regular FeN_6 octahedral environment in the LS state. $[Fe(phen)_2(NCS)_2]$ exhibits LIESST properties; a complete HS state was reached at 6 K by irradiation in the visible range using filtered white light or light from an He–Ne laser ($\lambda = 632.8$ nm) (Decurtins, Gütlich, Köhler & Spiering, 1985; Decurtins, Gütlich, Hasselbach *et al.*, 1985; Herber & Casson, 1986). A LIESST relaxation temperature of $T_{\rm LIESST} = 62$ K was characterized from photomagnetic measurements (Balde *et al.*, 2007). The structure of the HS-2 state of $[Fe(phen)_2(NCS)_2]$ was determined at 30 K by single-crystal diffraction under He–Ne laser light excitation and has been described in detail (Marchivie *et al.*, 2002). In addition, Lee *et al.* (2000) reported results from an X-ray absorption analysis of the HS-2 light-induced state. A comparison of the HS-2 crystal structure with that of the room-temperature HS-1 phase indicates a significant shortening of the Fe—N bond distances, together with a contraction of the intermolecular S···C and C···C contacts, probably due to thermal effects.

The present paper is organized as follows. §2 describes the X-ray diffraction measurements and the corresponding structural refinements. In §3, methodological aspects of photo-crystallographic studies are detailed, in particular the adequacy of CCD area detectors for such studies, and the influence of relaxation (or incompleteness of the photo-conversion) on the precision of the structural parameters are discussed. We finally propose an approach to improve the precision of crystal structure parameters refined for metastable states.

2. Diffraction measurements and structural refinements

Several sets of X-ray diffraction measurements were performed on $[Fe(phen)_2(NCS)_2]$ in the LS and light-induced metastable HS-2 states. In a first step, two data collections were performed at $T = 32$ K, using laboratory equipment. The experimental conditions we used proved to be not completely satisfactory and after structural refinement, biases in the structural parameters were discovered. Complementary and

Table 1
Crystallographic data and experimental details.

	32 K HS-2	32 K LS	15 K HS-2	15 K LS
Crystal system	Orthorhombic	Orthorhombic	Orthorhombic	Orthorhombic
Space group	*Pbcn*	*Pbcn*	*Pbcn*	*Pbcn*
a (Å)	13.1928 (4)	12.7408 (8)	13.185 (1)	12.762 (1)
b (Å)	9.9503 (3)	10.0227 (17)	9.948 (1)	10.024 (1)
c (Å)	17.1498 (8)	17.1166 (11)	17.135 (1)	17.090 (1)
V (Å^3)	2251.3 (1)	2185.7 (4)	2247.5 (3)	2186.2 (3)
Z	4	4	4	4
Crystal size (mm)	0.15 × 0.10 × 0.05	0.25 × 0.11 × 0.10	0.24 × 0.22 × 0.21	0.24 × 0.22 × 0.21
X-ray source	Sealed tube (Mo $K\alpha$)	Sealed tube (Mo $K\alpha$)	Synchrotron	Synchrotron
λ (Å)	0.71073	0.71073	0.71	0.71
Max. $\sin\theta/\lambda$ (Å^{-1})	0.80	0.81	1.00	1.00
Scan type	ω scan	ω scan	Φ scan	Φ scan
Limiting indices	$0 < h < 20$	$0 < h < 19$	$0 < h < 26$	$0 < h < 25$
	$0 < k < 15$	$0 < k < 13$	$0 < k < 19$	$0 < k < 20$
	$0 < l < 22$	$0 < l < 26$	$0 < l < 31$	$0 < l < 31$
No. of measured reflections	18028	3960	23123	23007
No. of independant reflections	4045	2551	7259	7122
Completeness (%)	82.6	51.7	72.2	77.3
R_{int}	0.055	0.063	0.021	0.019
Parameters/restraints	191/0	*	191/0	191/0
*R*1 (all data)	0.0986	*	0.0879	0.0665
*wR*2 (all data)	0.1083	*	0.1995	0.1482
GoF (all data)	0.908	*	1.066	1.034

* The 32 K LS data set was collected solely as an experimental control.

more accurate data were then collected at the ESRF (Grenoble, France) at T = 15 K, using improved laser excitation conditions. Accordingly, the laboratory 32 K data sets offer the opportunity to quantify the biases in the structural parameters by comparison with the 15 K structures. Details concerning the data collections and refinement results are collected in Table 1. The molecular structure of the HS-2 state at 15 K is given in Fig. 1.

2.1. Laboratory 32 K data collections

Single crystals of $[Fe(phen)_2(NCS)_2]$ of good quality were obtained by slow solvent-diffusion methods (Gallois *et al.*, 1990). Well shaped samples were selected for the diffraction measurements, embedded in vacuum grease and mounted on a glass fibre. Data were collected in the LS and HS-2 states, using, in Nancy, an Oxford Diffraction Xcalibur diffractometer equipped with a CCD area detector and an He open-flow Helijet cryosystem. The temperature was calibrated at the sample position, using the tetragonal to orthorhombic phase transition of a $DyVO_4$ sample at 14 K (Forsyth & Sampson, 1971).

The unit-cell parameters were recorded against the temperature, starting from room temperature in the HS state down to 32 K in the LS state, passing through the thermal HS–LS transition. In a second step, the HS-2 state was laser-excited at 32 K from LS, and then the temperature was increased until the HS-2 to LS relaxation occurred. The results are shown in Fig. 2.

A complete data set was collected for the light-induced HS-2 state at T = 32 K. Measurement conditions such as excitation power, excitation duration, continuous/pulsed excitation,

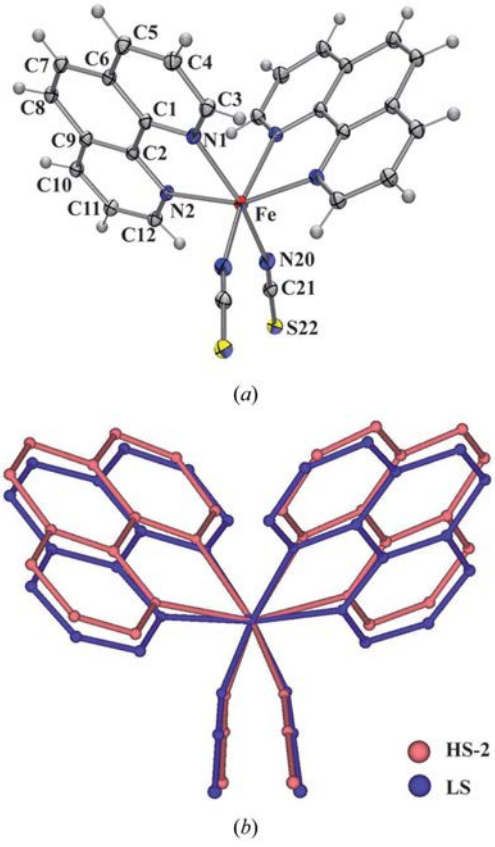

Figure 1
(*a*) Molecular structure and labelling scheme of $[Fe(phen)_2(NCS)_2]$ in the HS-2 state (T = 15 K). Thermal displacement ellipsoids (Johnson, 1976) are drawn at the 50% probability level. (*b*) Superposition of the LS and HS-2 molecular structures (derived from the 15 K data sets); H atoms are omitted.

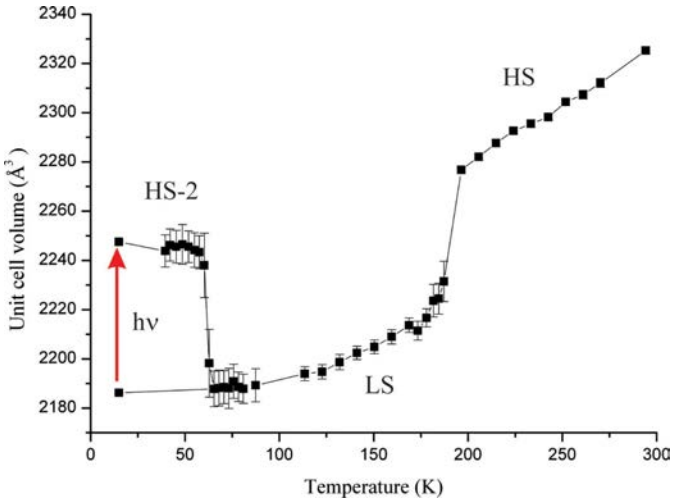

Figure 2
Unit-cell volume and spin state as a function of temperature (15 K < T < 298 K) and light irradiation.

wavelength of the light source and temperature, were all chosen according to previously published spectroscopic and photo-magnetic results. The electronic spectrum of $[Fe(phen)_2(NCS)_2]$ in the LS state shows a band at 960 nm attributed to the $^1A_1 \rightarrow {}^3T_1$ transition, and an intense band at 580 nm due to a ^{1}MLCT (metal to ligand charge transfer) transition (König & Madeja, 1967). To reach a large photo-induced metastable HS-2 population, the light penetration depth should be large enough to pass through the single-crystal sample. However, to our knowledge, as the wavelength dependence of the linear absorption coefficient has not been determined for this compound, it is impossible to calculate the penetration depth. According to the dark red colour of the samples, a high absorption is expected in the visible range, certainly due to the intense MLCT band. A wavelength of 647 nm (Ar–Kr gas laser), next to the maximum of absorption at 580 nm, was chosen as a compromise to ensure at the same time a deep light penetration and a large excitation efficiency. Marchivie *et al.* (2002) used a similar wavelength (647 nm) in their photo-crystallographic experiments for the same reasons. The laser power is a very important tunable parameter, the optimum value of which is hard to estimate. In the mean field approximation, following Enachescu *et al.* (Enachescu *et al.*, 2001; Varret *et al.*, 2004), the macroscopic evolution equation is written as

$$\frac{d\gamma_{HS}}{dt} = \Phi_{\text{photo-excitation}} - \Phi_{\text{relaxation}} = I^{\text{eff}}\sigma(1-\gamma_{HS}) - \gamma_{HS}k_{HL}(T,\gamma_{HS}), \quad (1)$$

where γ_{HS} is the fraction of HS species. The first term on the right-hand side is the linear photo-conversion rate, written as the product of the irradiation light intensity I^{eff} and a response factor σ depending on the absorption cross section and the quantum yield of the photo-excitation process. The second term corresponds to the HS to LS self-accelerated relaxation with relaxation rate constant $k_{HL}(T,\gamma_{HS})$. The fraction of HS species γ_{HS} at the photo-stationary state is therefore directly related to the light intensity, and, accordingly, a laser power as high as possible would be required to maximize γ_{HS} at saturation. On the other hand, the temperature increase in the single-crystal sample, released by thermalization of the photo-induced state and phonon emission, could be quite high and damage the crystal. The laser power should thus be tuned carefully to prevent this temperature increase. As the required laser power is hard to estimate, an empirical procedure has been proposed by Legrand *et al.* (2007). In the present situation, the optimum laser power, laser wavelength and excitation duration were determined empirically from several trial runs.

The mounted crystal was first cooled to 32 K by flash cooling to prevent damage occurring during the thermal transition. This particular temperature was chosen well below T_{LIESST} because the relaxation rate of $[Fe(phen)_2(NCS)_2]$ is temperature dependent and decreases drastically with temperature (Balde *et al.*, 2007). It was found for other spin-crossover materials, such as $[Fe(PM\text{-}BiA)_2(NCS)_2]$ (Marchivie *et al.*, 2004) or $[Fe(btr)_2(NCS)_2].H_2O$ (Legrand *et al.*, 2006), that such a cooling procedure can quench the system in a metastable HS-2 state. This is not the case for $[Fe(phen)_2(NCS)_2]$, as shown by a short data collection at T = 32 K just after flash cooling, which ensured that the cell parameters and Fe—N bond distances were indeed consistent with an LS state ($d_{Fe-N} \simeq 2.0$ Å). The single crystal was then exposed for 150 s to the 647 nm excitation light (50 mW) while the sample was continuously rotated to ensure a spatially homogeneous excitation. Lattice parameters were then determined, and indicated an LS to HS-2 photo-induced transition. A complete set of X-ray diffraction data were then collected over nearly 22 h with the sample in the light-induced HS-2 state, with an ω scan over 337°, a 1° frame width and 100 s exposure time per frame. Since at this temperature the HS-2 to LS relaxation is not negligible (see below), a laser excitation (647 nm, 50 mW) of 15 s was repeated every two hours. The photo-stationary state obtained with this excitation procedure is close to γ_{HS} = 1 during the whole measurement. The reflection profiles were integrated using the software package *CRYSALIS* (Oxford Diffraction, 2004). A Gaussian analytical absorption correction was then applied and the data also corrected empirically for vacuum-grease absorption (*SORTAV*; Blessing, 1989). In all, 18028 reflections were collected and merged into 4045 unique reflections, yielding a maximum resolution of $(\sin\theta/\lambda)_{\max}$ = 0.80 Å^{-1} and an overall completeness of 82.6%. The corresponding crystal structure was refined using *SHELX97* (Sheldrick, 1997). Non-hydrogen atoms were refined anisotropically; hydrogen atoms were refined isotropically without any constraint.

As mentioned above, a complementary and limited data set was also collected in the LS state at T = 32 K, using a 1° frame width and an exposure time of 60 s per frame. The data reduction procedure was the same as for the HS-2 case above. Data were merged, yielding 2551 unique reflections with a resolution of 0.81 Å^{-1} and a completeness of 51.7%. This data set was used solely to analyse the structural contrast between the LS and HS-2 states (see below).

2.2. Data collections at 15 K (ESRF, Grenoble)

The previous LS and HS-2 data collections were repeated using improved excitation conditions and an enhanced X-ray flux. This last condition was crucial owing to the small size of the available single crystals; the higher flux afforded an increase in the resolution of the data sets. Since the HS-2 to LS relaxation is central to our structural analysis, a lower temperature (T = 15 K) than for the laboratory case (T = 32 K) was chosen. The relaxation term in equation (1) is therefore further reduced; hence we expected a photo-stationary state with higher conversion throughout the diffraction measurements.

Data were collected on beamline BM01A at the ESRF, using a KUMA six-circle diffractometer equipped with an Onyx (Oxford Diffraction) CCD area detector and a Helijet cryosystem. Two detector positions (2θ equal to 50 and 130°) were used with a scan width $\Delta\varphi = 1°$ and a 4 s exposure time per frame. This gave us a higher resolution than in the laboratory. However, due to the shadowing of the detector by the Helijet nozzle, the completeness is reduced to 77.3% (LS state) and 72.2% (HS state) for the whole 2θ range, but as high as 97% and 96%, respectively, up to a resolution of 0.8 Å^{-1}.

For the metastable HS-2 state, the excitation was performed with an He–Ne laser operating at 1.25 mW. At this laser power, the temperature increase in the sample is almost negligible. Since the HS-2 to LS relaxation was not nearly as negligible if excitation took place every two hours, laser excitation was applied continuously.

The diffraction profiles from both HS-2 and LS data sets were integrated using *CRYSALIS* and Gaussian analytical absorption corrections were applied. The crystal structures were refined with *SHELX97*. Non-hydrogen atoms were refined anisotropically; hydrogen atoms were refined isotropically without any constraint, the same strategy than that used for the laboratory data.

Fig. 1(*b*) illustrates the structural reorganization related to the LS to HS-2 photo-conversion. In qualitative agreement with Marchivie *et al.* (2002), we observe an elongation of all Fe—N bonds and a less regular FeN_6 octahedral environment. As shown in Table 2, the quantitative agreement between the HS-2 states is, however, less satisfactory, with differences in the Fe—N bond lengths up to 0.032 Å, several times larger than the corresponding estimated standard deviations. Such differences among the three crystal structures of the HS-2 state exhibit some systematic variations and may stem from different γ_{HS} values at the photo-stationary state, as discussed below.

Table 2
FeN_6 octahedron geometry as a function of the spin state and the data origin.

V_p is the volume of the FeN_6 polyhedron (calculated using *IVTON*; Balic Zunic & Vickovic, 1996). Σ is the angular deformation of the FeN_6 octahedron, defined as the sum of the deviations from 90° of the 12 *cis* N—Fe—N angles in the coordination sphere (Guionneau *et al.*, 2004).

	32 K HS-2 (before LS species extraction)	32 K HS-2 (after LS species extraction)	30 K HS-2 (Marchivie *et al.*, 2002)	15 K HS-2	15 K LS
d_{Fe-N1} (Å)	2.207 (2)	2.211 (1)	2.184 (4)	2.216 (1)	1.980 (1)
d_{Fe-N2} (Å)	2.200 (2)	2.204 (1)	2.177 (4)	2.201 (1)	1.993 (1)
d_{Fe-N20} (Å)	2.085 (2)	2.088 (1)	2.066 (5)	2.083 (1)	1.936 (1)
Σ (°)	68.6 (8)	69.1 (8)	64 (2)	68.9 (6)	35.1 (5)
V_p (Å^3)	13.04 (2)	13.10 (2)	12.71 (6)	13.10 (1)	10.12 (1)

3. Results and discussion

3.1. HS-2 to LS relaxation process assessed from the diffraction pattern

If the unit-cell parameters of the metastable state are significantly different with respect to those of the ground state, it is common practice to rely on one cell parameter or on the cell volume to estimate the completeness of the ground to metastable state conversion (Legrand, 2005; Thompson *et al.*, 2004). Such a procedure is indeed quite common for spin-crossover systems; these exhibit in general large LS–HS cell-parameter changes which directly correlate with the fraction of HS species γ_{HS}. The evolution of the unit-cell volume during the course of the data collection of the metastable state could similarly yield an estimate of the relaxation kinetics, or at least a check on the significance of relaxation processes during the measurement. This method has been used with success during the X-ray diffraction measurements of the metastable state of the spin-crossover complex $[Fe(btr)_2(NCS)_2].H_2O$ (Legrand *et al.*, 2006). It should be noted that the photo-conversion kinetics can also be estimated from the time evolution of the measured intensity of several well chosen Bragg reflections (Honda *et al.*, 1999).

In the case of $[Fe(phen)_2(NCS)_2]$, the relaxation kinetics were determined from photo-magnetic and reflectivity measurements (Balde *et al.*, 2007). The relaxation rates were fitted to the self-acceleration formula proposed by Hauser (1992), $k_{HL}(T, \gamma_{HS}) = k_{HL}(T)\exp[\alpha(T)(1-\gamma_{HS})]$ with $k_{HL}(T) = k_{HL}(T \rightarrow 0) + k_{HL}(T \rightarrow \infty)\exp(-E_a/k_B T)$. The first term on the right hand side of $k_{HL}(T)$ corresponds to the tunnel regime with $k_{HL}(T \rightarrow 0)$ of 9.6×10^{-6} s^{-1}, while the second term corresponds to the thermally activated regime with activation energy E_a of 960 cm^{-1} and pre-exponential factor $k_{HL}(T \rightarrow \infty)$ of 1.0×10^7 s^{-1}. These relaxation rates indicate that even if we perform diffraction measurements at very low temperature, a significant relaxation during the whole diffraction data collection may not be completely negligible. This aspect has been investigated for the HS-2 laboratory measurement at 32 K in which the laser excitation was repeated every 2 h during data collection. The time between two successive excitations has been divided into seven shells of identical duration Δt (Δt = 120/7 min): $(0 \rightarrow \Delta t)$, $(\Delta t \rightarrow 2\Delta t), \ldots, (6\Delta t \rightarrow 7\Delta t)$. The reflections measured in each shell (nearly 770) have been grouped and the corresponding cell parameters derived using *CRYSALIS*. In that way, we obtain the time dependence of the unit-cell parameters between two laser excitations. Assuming a linear dependence of the cell volume with γ_{HS}, the cell volume at time t can be approximated by

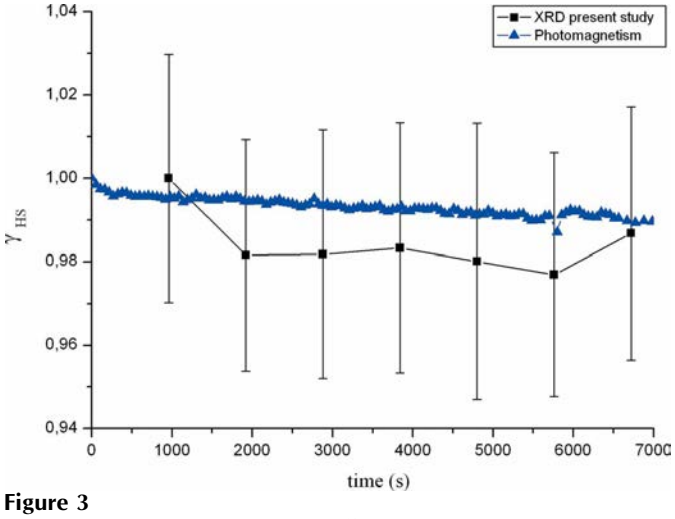

Figure 3
Evolution of the HS fraction $\gamma_{HS}(t)$ between two laser excitations: (squares) derived from our diffraction data using equation (2); (triangles) photo-magnetic measurements (Balde *et al.*, 2007). Standard deviations are derived from the diffraction data.

$$V(t) = \gamma_{HS\text{-}2}(t)\, V_{HS\text{-}2} + [1 - \gamma_{HS\text{-}2}(t)]\, V_{LS}, \qquad (2)$$

where $V_{HS\text{-}2}$ and V_{LS} correspond to the volume of purely HS-2 and LS states, respectively. V_{LS} is known from the purely LS-state measurement at 32 K; it amounts to 2185.7 Å^3. $V_{HS\text{-}2}$ has been estimated from the linear fit of $V(t)$ extrapolated to γ_{HS} = 1.0 and it amounts to 2251 Å^3. Knowing $V_{HS\text{-}2}$ and V_{LS} and measuring $V(t)$, the $\gamma_{HS}(t)$ curve can be easily derived from equation (2), and is given in Fig. 3 together with the photo-magnetic results. The value of $\gamma_{HS}(t)$ thus derived from our diffraction data is consistent with the photo-magnetic results and indicates a small but significant relaxation between the two-hourly laser excitations. The two-hour repetition rate of the laser excitation used during our laboratory measurement of the HS-2 state is therefore probably not sufficiently short to prevent significant relaxation. Better experimental conditions require a continuous laser excitation during data collection, as performed for the synchrotron 15 K HS-2 measurements. To summarize, the crystal structure derived from these 32 K data may be slightly erroneous since the probed system is continuously evolving during data collection.

The direct proportionality between the refined unit-cell volume (and cell parameters) and γ_{HS} [equation (2)] is verified especially for spin-crossover materials exhibiting gradual thermal transitions (Kusz *et al.*, 2000, 2001); it is the basis for the thermal expansion model (Spiering *et al.*, 1982; Adler *et al.*, 1987). The situation is more complex in the case of highly cooperative spin-crossover materials exhibiting abrupt spin transition, characterized by a heterogeneous mechanism and phase separation (HS and LS) (Pillet *et al.*, 2004, 2006; Huby *et al.*, 2004). The corresponding diffraction pattern for a mixed spin state ($0.0 < \gamma_{HS} < 1.0$) exhibits well separated Bragg peaks which can be indexed on the basis of the LS and HS-2 crystal lattices (Pillet *et al.*, 2004). In such a case, the refined cell parameters and cell volume depend strongly on the peak indexing procedure and no longer follow a linear relationship with γ_{HS}. For $[Fe(phen)_2(NCS)_2]$, which indeed exhibits Bragg peak splitting, the cell parameters were derived using the *CRYSALIS* software by a least-squares optimization refinement (Paciorek *et al.*, 1999). To quantify the possible bias in the refined cell parameters, which could result from the Bragg peak elongation or splitting during the relaxation, we simulated the diffraction pattern for given values of γ_{HS} ($0.0 \leq \gamma_{HS} \leq 1.0$ by 0.1 steps) in the following way: ten frames (frame width 1°) were collected in the pure HS-2 and LS states, covering exactly the same region of reciprocal space in both spin states. A typical diffraction frame consists of an array of 512 × 512 pixels. Then for each value of γ_{HS}, the same reciprocal-space region (ten frames) was simulated as a weighted sum, pixel by pixel, of the diffraction frames of the pure HS-2 (weighted by γ_{HS}) and LS states (weighted by $1 - \gamma_{HS}$). Fig. 4 gives an example of such a simulated diffraction pattern for γ_{HS} = 0.8. The cell parameters and cell volume were refined for each simulated γ_{HS} data set, using *CRYSALIS*; the corresponding volume was converted to γ_{HS} values, using equation (2). In Fig. 5, the obtained values of γ_{HS} are reported against the reference γ_{HS} used for the construction of the

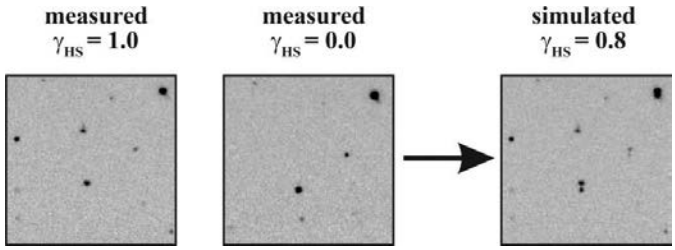

Figure 4
Simulation of the mixed-crystal diffraction pattern for γ_{HS} = 0.8. Black spots are the Bragg peaks. The diffraction frames of the mixed crystal have been obtained by a direct weighted sum of the HS-2 and LS experimental diffraction frames at 32 K: $P_{i,j}(\gamma_{HS} = 0.8) = 0.8P_{i,j}(\gamma_{HS} = 1.0) + 0.2P_{i,j}(\gamma_{HS} = 0.0)$ where $P_{i,j}$ is the value of the (i, j) pixel of the diffraction frame. Note the Bragg peak splitting for the mixed crystal.

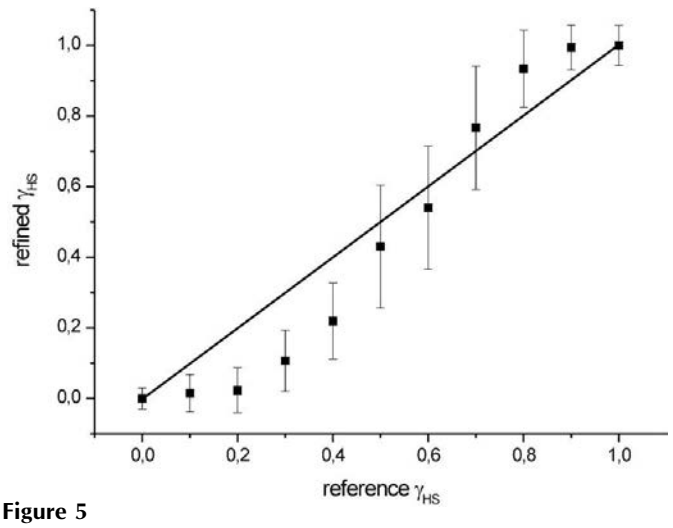

Figure 5
Comparison between γ_{HS} derived from the cell-parameter refinement (square) and the reference γ_{HS} (line) used for the simulation of the corresponding diffraction frames.

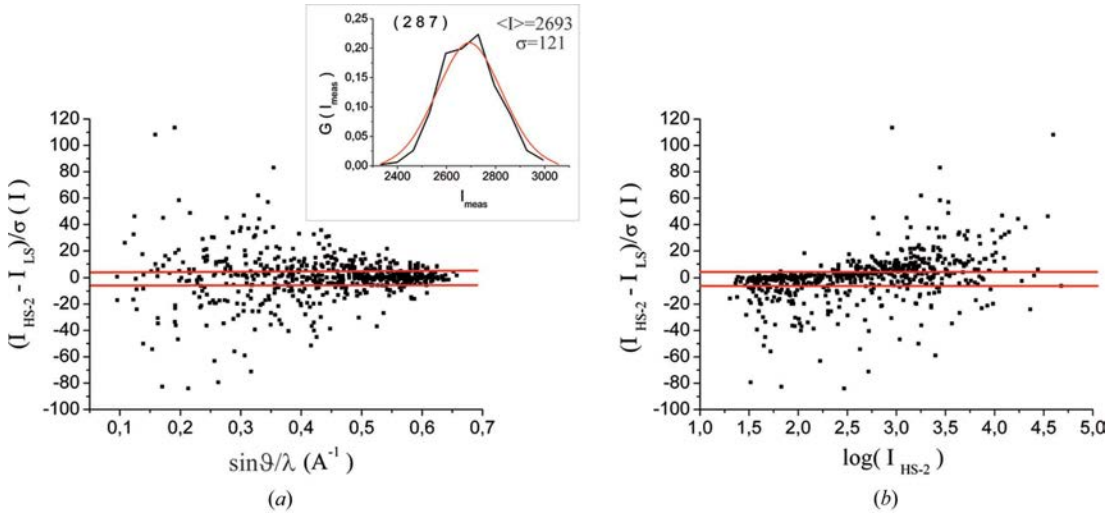

Figure 6
Contrast factor $(I_{\text{HS-2}} - I_{\text{LS}})/\sigma(I)$ as a function of (*a*) resolution $\sin(\theta)/\lambda$ and (*b*) $\log(I_{\text{HS-2}})$. Inset: intensity distribution of the 287 reflection. Horizontal lines are at the $(I_{\text{HS-2}} - I_{\text{LS}})/\sigma(I) = \pm 3$ level.

simulated diffraction frames. Instead of a linear correlation with unit slope, we observe a sigmoidal dependence, indicating that a bias is indeed introduced across the whole γ_{HS} range; it is even more spectacular at the early and late stages of the relaxation.

This simulation shows that the procedure for deriving $\gamma_{\text{HS}}(t)$ from the evolution of the cell volume should be used with care when using conventional peak indexing programs. Although it can be efficient in the case of weakly cooperative systems with gradual spin transition (without Bragg peak splitting), it is inappropriate for strongly cooperative systems for which the spin transition occurs heterogeneously through phase separation characterized by a Bragg peak elongation or splitting. This is exactly the case for $[Fe(phen)_2(NCS)_2]$, which exhibits a clear separation of Bragg peaks at the spin transition, especially for *h*00-type reflections, since the *a* cell parameter is the one that changes most at the transition. Our simulation demonstrates the need for an external means of determining the HS–LS relaxation in parallel with the diffraction measurement. Such a device is now under development in our laboratory.

3.2. Structural contrast and suitability of CCD area detectors for photo-crystallographic experiments

The use of CCD area detectors is widespread in the field of photo-crystallography since, for equal measurement time, many more Bragg reflections can be collected on a single frame than with a conventional point detector. It is often believed that the speed-up in data collection compensates for the loss of accuracy with respect to a point detector. We would like to address this question in the present section by analysing the contrast factor $(I_{\text{HS-2}} - I_{\text{LS}})/\sigma(I)$ for $[Fe(phen)_2(NCS)_2]$. The structural information we can obtain from a photo-crystallographic experiment is of course highly dependent on the accuracy of the measurement and therefore on the quality of the equipment. To obtain a clear estimate of the intrinsic accuracy of our CCD detector, we collected 30 frames (1° frame width) at room temperature on a single crystal of $[Fe(phen)_2(NCS)_2]$ and obtained 632 unique reflections. This measurement was repeated 500 times to yield reasonable statistics. For each unique reflection, which is therefore measured 500 times, the intensity distribution was plotted and the root mean square deviation (r.m.s.d.) of the distribution derived according to the formula

$$\sigma(I) = \left\{ \frac{\sum_i [1/\sigma^2(I_i)]\,(I_i - \langle I \rangle)^2}{\sum_i [1/\sigma^2(I_i)]} \right\}^{1/2}, \qquad (3)$$

where $\langle I \rangle$ is the mean intensity of the considered reflection, $\sigma^2(I_i)$ is estimated from the *CRYSALIS* software and the sum is performed over the 500 replicate intensities I_i.

For example, the intensity distribution of the 287 Bragg reflection is given in Fig. 6 (inset), the analysis of which leads to $\langle I \rangle = 2693$ and $\sigma(I) = 121$. This analysis yields the best estimate for the intensity standard deviation $\sigma(I)$. These r.m.s.d. values have been used after scaling to plot the contrast factor $(I_{\text{HS-2}} - I_{\text{LS}})/\sigma(I)$ as a function of $\log(I_{\text{HS-2}})$ and $\sin\theta/\lambda$ (Fig. 6) for the 32 K data collection. Large values of the contrast factor are observed for many reflections, spread over the whole intensity range and mostly in low and medium resolution range. This is due to the fact that large structural modifications occur during the photo-excitation of the LS state to HS-2. More than 59% of the reflections exhibit contrast values greater than three standard deviations. Then, using such a CCD area detector is justified as a good compromise between shortening of data collection time (to avoid significant relaxation) and accuracy.

3.3. Bias in the structural analysis of metastable states

When one aims to determine the crystal structure of a light-induced metastable state, it is often assumed that the photo-induced metastable state has a lifetime compatible with X-ray

diffraction techniques, if this lifetime is greater than, say, a few hours (Niel *et al.*, 2005; Ichiyanagi *et al.*, 2006). We will show in this section that if this assumption is not carefully checked, the refinement may lead to large biases in the derived structural parameters, which we will now quantify. Such a bias is of utmost importance if the corresponding bond distances are benchmarks for theoretical calculations. The situation may also apply to a slightly incomplete photo-conversion. To take into account such a relaxation effect, Pressprich *et al.* (1993) implemented a time dependence of the photo-induced species concentration during the refinement of the metastable state of sodium nitroprusside dihydrate from single-crystal diffraction measurements. In their least-squares refinement, they used a time dependence of the metastable and ground-state molecular occupancy factors instead of refining them as in a conventional treatment of a static disorder. A different strategy, adapted from the treatment of time-resolved spectroscopic data, was used for the analysis of the photo-induced dimerization of a cinnamic acid derivative by a powder diffraction technique (Busse *et al.*, 2002).

To test the influence of the relaxation on the refined structural parameters for $[Fe(phen)_2(NCS)_2]$, another simulation was performed, using the purely HS-2 and LS crystal structures as references. We considered the system as a random distribution of γ_{HS} fraction of HS-2 molecules and $(1 - \gamma_{HS})$ fraction of LS molecules, and generated 18 hypothetical mixed structures with $0.05 \leq \gamma_{HS} \leq 0.99$. For a random distribution, the asymmetric unit is built directly from a weighted superposition of the HS-2 molecular structure (with weight γ_{HS}) and the LS structure (with weight $1 - \gamma_{HS}$) (Vorontsov & Coppens, 2005). The 18 static intensity data sets were computed according to the formula

$$F^2(\gamma_{HS}) = [\gamma_{HS} F_{HS\text{-}2} + (1 - \gamma_{HS}) F_{LS}]^2, \qquad (4)$$

where $F(\gamma_{HS})$ is the structure-factor amplitude at a given γ_{HS} value, and $F_{HS\text{-}2}$ and F_{LS} correspond to the static structure factors of purely HS-2 and LS states, respectively. Note that for cooperative systems, the HS to LS transition occurs through phase separation, and the sum of the intensities, rather than the structure factors, would be required in equation (4) (Vorontsov & Coppens, 2005). The data sets have been generated with the same resolution and reciprocal-space coverage as in the experimental 32 K HS-2 measurement, *i.e.* 0.8 $Å^{-1}$, to be representative of a real measured data set. The structures corresponding to each of the 18 data sets have been refined by least squares, using *SHELX97*, and naively assuming a purely HS-2 state. This procedure reproduces the case for which a HS-2 to LS relaxation (or incompleteness of the LS to HS-2 conversion) occurs but is ignored in the structural refinement. The agreement indices at convergence of these structural refinements (given in supplementary material)[1] clearly indicate an inconsistency in most of the refined models as γ_{HS} approaches 0.5 with values as high as $R1 = 0.2169$ for $\gamma_{HS} = 0.5$.

The structural parameters (atomic positions and atomic displacement parameters) correspond to the refined HS-2 structure biased by the presence of the residual $(1 - \gamma_{HS})$ LS species. Using this simulation procedure for γ_{HS} ranging from 0.99 to 0.05, we are able to probe the influence of the residual LS species on the HS-2 refined structural parameters. In the following, we quantitatively analyse the biases introduced in commonly reported spin-crossover structural parameters such as Fe—N bond distances, FeN_6 polyhedron volume V_p and Σ angular distortion (Guionneau *et al.*, 2004). In addition, we calculated the atomic position misfit (mfa) as the mean position deviation between the refined atomic positions and the reference ones in the $\gamma_{HS} = 1$ structure (Hundt *et al.*, 2006).

We observe that for γ_{HS} ranging from 0.99 to 0.05, the refined crystal structure is indeed intermediate between the purely HS-2 and LS structures, as shown in Fig. 7. Not surprisingly, perturbation in the molecular structure is continuous between the reference $\gamma_{HS} = 1.0$ and $\gamma_{HS} = 0.0$ structures. The refined atomic positions are therefore highly biased by the residual LS species as these are not strictly taken into account in the structural refinement. The more surprising point, however, is that even a very small residue perturbs the structure refinement. This is illustrated in Fig. 8 which plots the residual electron density (Fourier transform of the difference between observed and calculated structure factors) and the corresponding 'peanut' representation of the atomic displacement differences for $\gamma_{HS} = 0.95$. At convergence of the refinement ($R1 = 0.029$), residual electron density peaks are observed at the positions corresponding to the 5% LS species. These LS residual densities should also produce a parallel bias in the refined atomic displacement parameters, and this is exactly what we observe in Fig. 8(*b*). All the atomic displa-

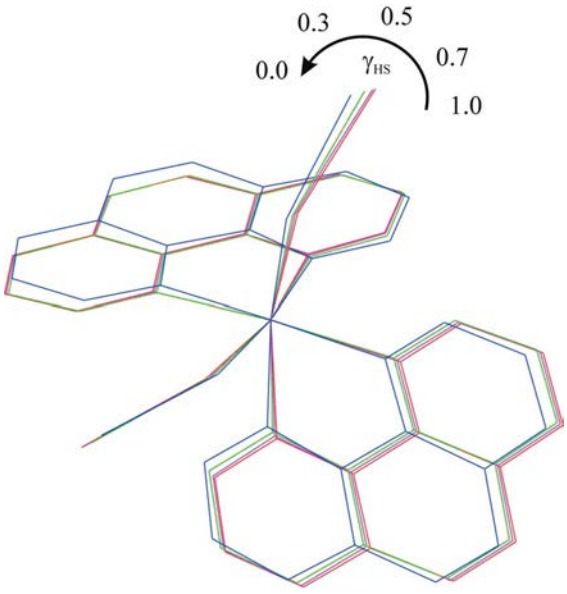

Figure 7
Superposition of the refined molecular structures for γ_{HS} = 1.0, 0.7, 0.5, 0.3 and 0.0.

[1] Supplementary data are available from the IUCr electronic archives (Reference: DB5028). Services for accessing these data are described at the back of the journal.

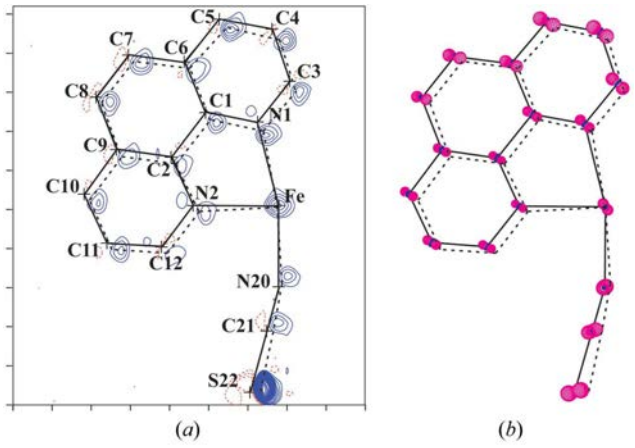

Figure 8
(*a*) Residual electron density after the structural refinement corresponding to γ_{HS} = 0.95 (contour spacing 0.2 e Å^{-3}; positive contours drawn in blue, negative ones in red, zero contour omitted for clarity). (*b*) *PEANUT* (Hummel *et al.*, 1990) plot of the mean-square displacement difference surfaces with arbitrarily exaggerated scale. The continuous black lines correspond to the refined molecular structure; the dashed lines belong to the purely LS molecular structure.

cement ellipsoids are elongated with their principal axis oriented towards the atomic positions of the pure LS structure. This is because the displacement parameters partly fit the residual electron density at the LS atomic positions, whether it is due to thermal motion, atomic disorder or both. One has to note that the origin of the displacement in the present situation can clearly be detected only because the simulated data sets consist of static structure factors; in a real case, atomic thermal motion would further smear out this residual electron density, rendering it almost featureless.

As for the atomic positions, the derived Fe—N bond lengths range continuously from the purely HS-2 value to the purely LS value (Figs. 9*a* and 9*b*). The effect is more pronounced for the Fe—N1 and Fe—N2 bonds than the Fe—N20 bond. Figs. 9(*c*) and 9(*d*) show the difference between the refined d_{Fe-N} and the reference d_{Fe-N} for γ_{HS} = 1.0 normalized by $\sigma(d_{Fe-N})$, the standard deviation for the γ_{HS} = 1.0 refined crystal structure. For γ_{HS} = 0.96 and lower, the bias is significant [$>3\sigma(d_{Fe-N})$]. This means that for a photo-stationary state of γ_{HS} = 0.96, or correspondingly for a mean 4% relaxation during the diffraction measurement, the derived Fe—N bond distances are significantly biased and the results obtained are quantitatively less meaningful. The effect is quite impressive. The curves plotted in Fig. 9 can be used as a benchmark to estimate the error of the refined Fe—N bond lengths for other spin-crossover materials. We highly recommended that this error be taken into account when discussing HS-2 to LS structural modifications or comparing HS-2 to HS-1 structures, which are currently much debated. We illustrate also in Fig. 9 the Fe—N bond lengths of the HS-2 metastable state reported by Marchivie *et al.* (2002) in their pioneering work. They used a single laser excitation at the beginning of their 9 h long data collection. Their bond lengths are systematically shorter than those obtained in the present analysis, for the 32 K as well as for the 15 K data sets. From an inspection of the reference curve of Fig. 9, we suspect their crystal structure to be biased by the residual LS species or by the HS-2 to LS relaxation. This must be the case as the relaxation of $[Fe(phen)_2(NCS)_2]$ over a period of 9 h is nearly 5% at 30 K. Therefore, the differences between HS-1 and HS-2 structures, especially in terms of Fe—N bond length, is less than claimed by Marchivie *et al.* (2002).

The FeN_6 polyhedron volume V_p (Fig. 10) and the Σ angular distortion parameters exhibit a similar continuous trend from the purely HS value to the purely LS one with nevertheless a jump for Σ from γ_{HS} = 0.05 to γ_{HS} = 0.0 (supplementary material). The standard deviation on the polyhedron volume is typically 0.01 Å^3 (in the 15 K HS-2 structure for instance). From γ_{HS} = 0.98 and lower, the bias in V_p becomes significant [bias > $3\sigma(V_p)$]. The Σ parameter is less affected than all the other structural characteristics, the bias being significant only from γ_{HS} = 0.9.

Fig. 11 gives the atomic position misfit (mfa) *versus* reference γ_{HS}, which indicates the mean error in the refined atomic positions that occurs if the residual LS population is ignored.

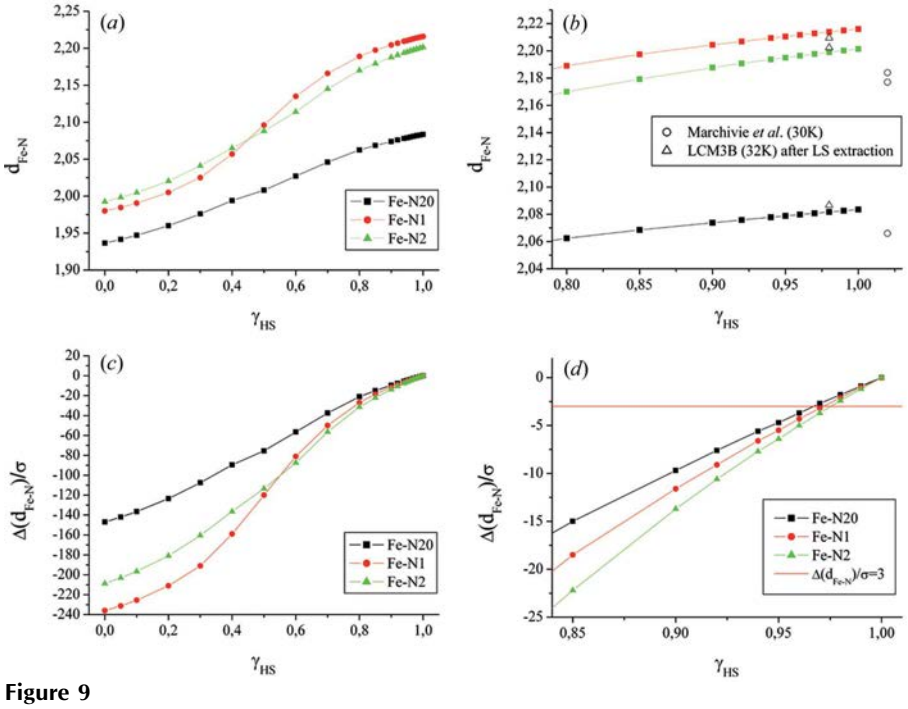

Figure 9
(*a*) Refined Fe—N bond lengths as a function of reference γ_{HS}. (*b*) Enlargement of (*a*) in the range $0.8 < \gamma_{HS} < 1.0$. (*c*) $[d_{Fe-N}(\gamma) - d_{Fe-N}(\gamma = 1.0)]/\sigma[d_{Fe-N}(\gamma = 1.0)]$ as a function of reference γ_{HS}. (*d*) Enlargement of (*c*) in the range $0.85 < \gamma_{HS} < 1.0$. Part (*b*) also shows d_{Fe-N} corresponding to the 32 K data set after extraction of the LS species ($\gamma_{HS} \simeq 0.98$) and to those of Marchivie *et al.* (2002) (unknown mean γ_{HS}).

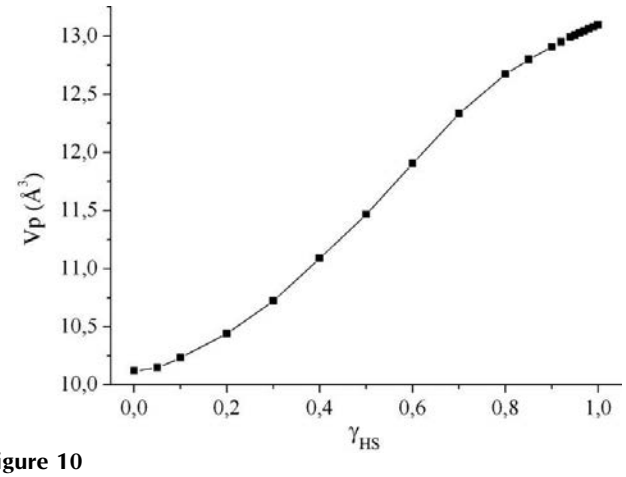

Figure 10
Volume V_p of the FeN_6 polyhedron as a function of reference γ_{HS} [V_p has been calculated using *IVTON* (Balic Zunic & Vickovic, 1996)].

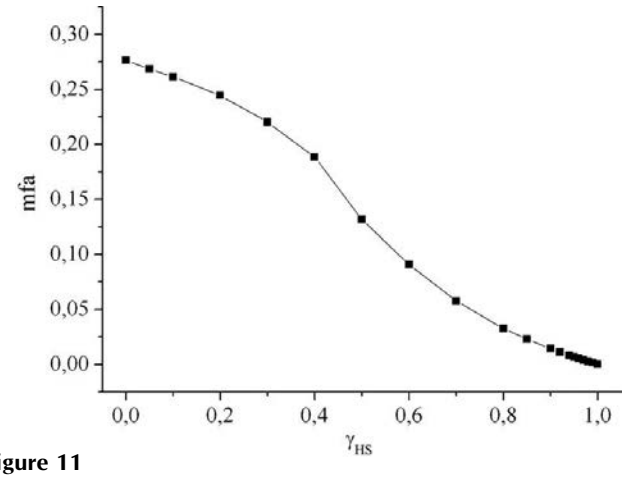

Figure 11
Atomic position misfit (mfa) as a function of reference γ_{HS}. mfa = $(\sum_{i=1}^{n} s_i^2/n)^2$, where s_i are the distances (in Å) between corresponding pairs of atoms in the refined and reference γ_{HS} = 1.0 structures. [mfa has been calculated using *KPLOT* (Hundt *et al.*, 2006).]

The value of mfa at γ_{HS} = 0.0 gives the mean atomic deviation between the LS and HS-2 molecular structures, which is as high as 0.276 Å. While reporting crystal structures refined by least-squares against photo-crystallographic data, the usual atomic position accuracy is in the range of a few 0.001 Å. For $\gamma_{HS} \leq 0.96$, the atomic position misfit exceeds 0.005 Å, and the bias on the atomic positions is larger than the estimated accuracy. In conclusion, the atomic position precision is lower than usually assumed. The mean contribution of this 'split atom' situation to the atomic displacement parameters discussed above may be approximated by

$$U_{split} = (1 - \gamma_{HS})\,(0.276 - \text{mfa})^2 + \gamma_{HS}\,\text{mfa}^2 \qquad (5)$$

and is valid only for mfa smaller than or close to 0.276, *i.e.* for small mean displacements with respect to the HS-2 or LS states (Ribbe *et al.*, 1969). A more elaborate model applied to an LS–HS transition is described by Chandrasekhar & Bürgi (1984). As an example, for γ_{HS} = 0.96, U_{split} = 0.003 Å^2, which is to be compared with U_{eq}(Fe) = 0.01252 (7) Å^2 in the HS-2 state at 15 K.

3.4. Improvement of the HS-2 metastable-state structural model

Using what we learned from the previous simulations, we tried to improve the precision of our refined HS-2 crystal structure at 32 K. The procedure consisted of using the known LS crystal structure to extract the HS-2 crystal structure from the measured data. We first illustrate the procedure on the simulated data sets discussed above and then on the laboratory 32 K data set which (we know) is affected by the HS-2 to LS relaxation. This approach is used almost routinely in the case of incomplete photo-conversion (see *e.g.* Kovalevsky *et al.*, 2005; Turowska-Tyrk, 2003; Enkelmann *et al.*, 1993; Bowes *et al.*, 2006) and is strictly valid only when the population of metastable- and ground-state species is not evolving during data collection time.

We first assess the contribution of the LS species on our measured Bragg intensities. The normalized structural contrast for γ_{HS} = 0.95 and γ_{HS} = 0.80 is illustrated in Fig. 12 as $[I(\gamma_{HS} = 0.95) - I(\gamma_{HS} = 1.00)]/I(\gamma_{HS} = 1.00)$ and (*b*) $[I(\gamma_{HS} = 0.80) - I(\gamma_{HS} = 1.00)]/I(\gamma_{HS} = 1.00)$ as a function of $I(\gamma_{HS} = 1.00)$. One can easily see that many reflections exhibit large differences between the LS and the HS-2 states, even for γ_{HS} = 0.95, owing to the large structural changes at the LS–HS transition. The weakest reflections exhibit the largest contrast factors. Spin-crossover molecular complexes are indeed good candidates for structural analysis of metastable states. A least-squares refinement should therefore be appropriate to extract separately the LS and HS-2 structures from these data. We used the γ_{HS} = 0.95 and γ_{HS} = 0.80 data sets simulated previously and modelled the crystal structures as a statistical superposition of the known LS molecular structure and the to-be-determined HS-2 structure. The previously refined and biased crystal structures assuming a purely HS-2 state (from §3.3) were taken as starting points. The LS molecular structure was transferred as a rigid group from the LS refinement and centred at the Fe atom position, since the LS and HS-2 cell parameters differ. The HS-2 to LS species ratio was refined as a molecular occupancy factor and the atomic positions of the LS state kept fixed. At convergence of the refinement using *SHELX97*, the occupancy factors were 0.95151 (2) and 0.79998 (1), in close agreement with 0.95 and 0.80. In addition, all the HS-2 structural parameters, Fe—N bond distances, V_p, and Σ are very close to the γ_{HS} = 1.0 reference values (Table 3). The corresponding refinement agreement indices are much reduced, from $R1$ = 0.0287 to $R1$ = 0.0009 and from $R1$ = 0.1128 to $R1$ = 0.0002 for γ_{HS} = 0.95 and γ_{HS} = 0.80, respectively. This shows that the procedure is indeed efficient in the cases illustrated.

A similar refinement strategy was tested on the 32 K crystal structure of the HS-2 state, using the 15 K LS molecular structure as reference. To stabilize the refinement, the atomic displacement parameters of the LS and HS-2 states were constrained to be identical, and a single atomic displacement parameter was refined for all H atoms. All x, y, z and U_{ij} parameters of the HS-2 state were refined together with the HS occupancy factor. At convergence, the occupancy factor

Table 3
Structural parameters obtained before and after LS species extraction for the γ_{HS} = 0.95 and γ_{HS} = 0.80 simulated data.

V_p and Σ are defined in Table 2.

	γ_{HS} = 0.95 (before extraction)	γ_{HS} = 0.95 (after extraction)	γ_{HS} = 0.80 (before extraction)	γ_{HS} = 0.80 (after extraction)	Reference structure (γ_{HS} = 1.0)
d_{Fe-N1} (Å)	2.210	2.216	2.189	2.216	2.216 (1)
d_{Fe-N2} (Å)	2.195	2.201	2.170	2.201	2.201 (1)
d_{Fe-N20} (Å)	2.079	2.083	2.062	2.083	2.083 (1)
Σ (°)	68.1	68.9	64.8	68.9	68.9 (6)
V_p (Å^3)	13.01	13.09	12.67	13.10	13.10 (1)

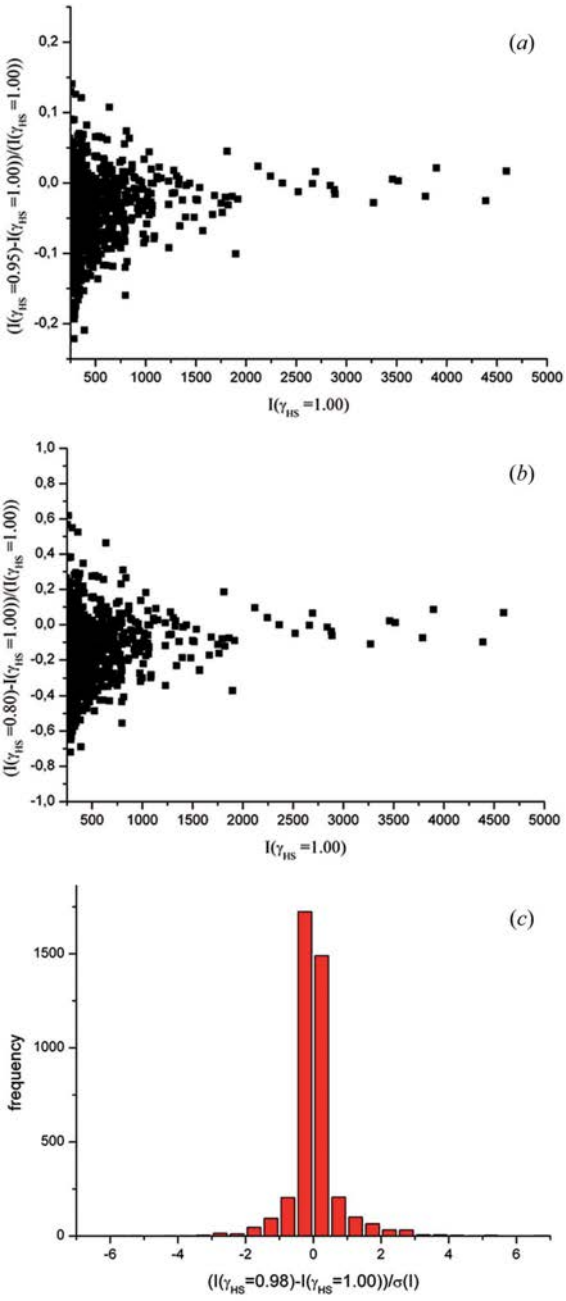

Figure 12
(*a*) $[I(\gamma_{HS} = 0.95) - I(\gamma_{HS} = 1.00)]/I(\gamma_{HS} = 1.00)$ and (*b*) $[I(\gamma_{HS} = 0.80) - I(\gamma_{HS} = 1.00)]/I(\gamma_{HS} = 1.00)$ as a function of $I(\gamma_{HS} = 1.00)$ for the simulated data. (*c*) Frequency plot of $[I(\gamma_{HS} = 0.98) - I(\gamma_{HS} = 1.00)]/\sigma(I)$ for the experimental 32 K data.

was highly significant 0.9776 (9), indicating a 2% mean relaxation between the two-hour laser excitation repetitions. This is in agreement with the value we have estimated from the cell-volume evolution (Fig. 3). Using this specific refinement procedure, the Fe—N bond lengths increase significantly from 2.207 (2), 2.200 (2) and 2.085 (2) Å to 2.211 (1), 2.204 (1) and 2.088 (1) Å [reported in Fig. 9(*b*) and Table 2], but the Σ and V_p parameters were barely affected.

The intensity contrast $[I(\gamma_{HS} = 0.98) - I(\gamma_{HS} = 1.00)]/\sigma(I)$ has been calculated from the refined structures at γ_{HS} = 0.98 and γ_{HS} = 1.0, using the corresponding experimental standard deviations $\sigma(I)$ from the 32 K HS-2 data set. The resulting distribution is given in Fig. 12(*c*). Most of the reflections are restricted to $|I(\gamma_{HS} = 0.98) - I(\gamma_{HS} = 1.00)| < \sigma(I)$, and very few reflections have a contrast greater than $3\sigma(I)$. In this situation, a refinement combining both spin-state molecular structures should be very hard to achieve, given the accuracy of our 32 K data set, but it was nevertheless successful as judged by the structural parameters evolution discussed above, even though the refinement agreement indices are barely affected: *R*1 decreases from 0.0986 to 0.0983 after LS-species extraction.

One might ask how it could be possible to detect from the raw diffraction data whether the measured photo-converted state actually corresponds to a truly complete metastable state, with no residual ground-state species, and for which relaxation is negligible. One efficient way would be to analyse the statistics of the $(F^2_{obs} - F^2_{calc})$ residues at convergence of the structural refinement (Abrahams & Keve, 1971). A non-Gaussian distribution of the residues would indicate that the structural model is not appropriate for the given diffraction data set. As an example, the normal probability plots corresponding to the laboratory 32 K HS-2 data set with the two structural models discussed above, namely with and without taking care of the 2% LS species, have been calculated (Fig. 13). These plots are almost identical; the relaxation is not severe enough in this case to be detectable by the statistics of the residues. However, we think this tool might be helpful in other situations.

4. Conclusion

We have reported a critical and quantitative analysis of the precision of crystal structures of light-induced metastable states derived from X-ray diffraction measurements, using the spin-crossover compound $[Fe(phen)_2(NCS)_2]$ as a repre-

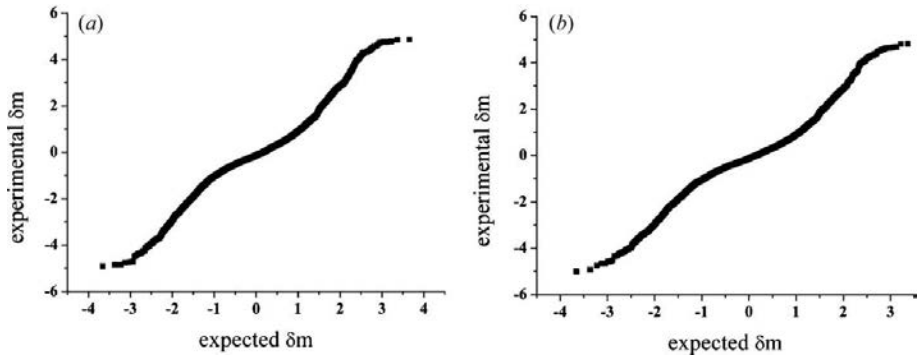

Figure 13
Normal probability plot of $\delta m = (F^2_{obs} - F^2_{calc})/\sigma(F^2_{obs})$ for the 32 K data set corresponding to (*a*) before extraction of the LS species and (*b*) after extraction of the LS species.

sentative example. To support our results, we have performed several complementary simulations. This permits us to make the following conclusions.

(i) Unit-cell parameters and volume are good indicators of the completeness of the ground to metastable state (light-induced) conversion or, in some cases, of the relaxation rate. In the case of highly cooperative systems, for which a Bragg peak splitting or an enlargement is observed in the diffraction pattern, the derived fraction of metastable to ground-state species is not quite as meaningful. The procedure, however, is relevant for weakly cooperative systems, which to our knowledge is the most common situation.

(ii) The intrinsic accuracy of CCD detectors is compatible with the intensity contrast between the ground state and the metastable state of a typical spin-crossover molecular system. This conclusion may not hold for other systems, since it is well known that spin-crossover materials undergo a large structural reorganization upon passing through the spin transition. The experimental setup used here may not be accurate enough for systems exhibiting only subtle structural or electronic changes. Alternative specific refinement or additional noise filtering techniques may prove helpful.

(iii) In the presence of residual ground-state species, the derived crystal structure assuming a complete metastable state is biased. In the presence of only a 4–5% residual ground-state population, the bias in bond lengths, polyhedron volume or, to a lower extent, angular structural parameters is significant. This unexpected but noteworthy influence of a small residue should be taken into account in future attempts to determine structure–property relationships. Indeed, it is well known that, for example, after the thermal conversion, residual HS species might still be present in the LS phase, and *vice versa*, depending on the thermal history of the sample, and could therefore cast some doubts on the accuracy of the structural discussions. The reference curves given in this work can be used as benchmarks to estimate the errors in similar studies. A prior determination of the ground-state structure at the same temperature can be used to extract and improve the crystal structure of the metastable state. Even when the structure of the metastable state seems reasonable and no residual ground-state species is suspected, as was the case with the 32 K structure of $[Fe(phen)_2(NCS)_2]$, the procedure leads to a significant improvement. It is expected that such biases occur even more frequently in time-resolved diffraction measurements. Accordingly, we recommend that diffraction studies of reversible photo-induced processes always be conducted under continuous laser excitation, even at the cost of a slight temperature increase (see also MacLean *et al.*, 2003). Care must be taken with highly temperature-dependent relaxation kinetics.

Summing up, we can state that by improving the experimental conditions, in particular the excitation procedure, we have been able to collect data of a quality high enough to render an electron density analysis of $[Fe(phen)_2(NCS)_2]$ in its light-induced metastable state possible. These results will be published in a forthcoming paper.

This work was financially supported by the European Network of Excellence MAGMANet (FP6-515767-2), the Université Henri Poincaré and the CNRS. VL is indebted to the Ministère de l'Education Nationale, de l'Enseignement Supérieur et de la Recherche for a doctoral fellowship. We thank the ESRF and the BM01A beamline staff for their support during the measurements of the 15 K data sets. One of the referees is gratefully acknowledged for improving the stylistic quality of our manuscript.

References

Abrahams, S. C. & Keve, E. T. (1971). *Acta Cryst.* A**27**, 157–165.
Adler, P., Wiehl, L., Meissner, E., Köhler, C. P., Spiering, H. & Gütlich, P. (1987). *J. Phys. Chem. Solids*, **48**, 517–525.
Balde, C., Desplanches, C., Degert, J., Freysz, E., Gütlich, P., Guionneau, P. & Létard, J.-F. (2007). To be published.
Balić Žunić, T. & Vicković, I. (1996). *J. Appl. Cryst.* **29**, 305–306.
Blessing, R. H. (1989). *J. Appl. Cryst.* **22**, 396–397.
Bowes, K. F., Cole, J. M., Husheer, S. L. G., Raithby, P. R., Savarese, T. L., Sparkes, H. A., Teat, S. J. & Warren, J. E. (2006). *Chem. Commun.* pp. 2448–2450.
Busse, G., Tschentscher, T., Plech, A., Wulff, M., Frederichs, B. & Techert, S. (2002). *Faraday Discuss.* **122**, 105–117.
Chandrasekhar, K. & Bürgi, H.-B. (1984). *Acta Cryst.* B**40**, 387–397.
Cole, J. M. (2004). *Chem. Soc. Rev.* **33**, 501–513.
Collet, E., Lemée-Cailleau, M. H., Buron-Le Cointe, M., Cailleau, H., Wulff, M., Luty, T., Koshihara, S. Y., Meyer, M., Toupet, L., Rabiller, P. & Techert, S. (2003). *Science*, **300**, 612–615.
Coppens, P. (1992). *Synchrotron-Radiation Crystallography*, with contributions from D. E. Cox, E. Vlieg & I. K. Robinson, pp. 143–146. London: Academic Press.
Coppens, P., Novozhilova, I. & Kovalevsky, A. (2002). *Chem. Rev.* **102**, 861–883.
Coppens, P., Vorontsov, I. I., Graber, T., Gembicky, M. & Kovalevsky, A. Y. (2005). *Acta Cryst.* A**61**, 162–172.
Davaasambuu, J., Durand, P. & Techert, S. (2004). *J. Synchrotron Rad.* **11**, 483–489.
Decurtins, S., Gütlich, P., Köhler, C. P. & Spiering, H. (1984). *Chem. Phys. Lett.* **105**, 1–4.

Decurtins, S., Gütlich, P., Hasselbach, K. M., Hauser, A. & Spiering, H. (1985). *Inorg. Chem.* **24**, 2174–2178.
Decurtins, S., Gütlich, P., Köhler, C. P. & Spiering, H. (1985). *J. Chem. Soc. Chem. Commun.* pp. 430–432.
Enachescu, C., Constant-Machado, H., Codjovi, E., Linares, E., Boukheddaden, K. & Varret, F. (2001). *J. Phys. Chem. Solids*, **62**, 1409–1422.
Enkelmann, V., Wegner, G., Novak, K. & Wagener, K. B. (1993). *J. Am. Chem. Soc.* **115**, 10390–10391.
Forsyth, J. B. & Sampson, C. F. (1971). *Phys. Lett.* **36A**, 223–224.
Friscic, T. & MacGillivray, L. R. (2005). *Z. Kristallogr.* **220**, 351–363.
Fullagar, W. K., Wu, G., Kim, C., Ribaud, L., Sagerman, G. & Coppens, P. (2000). *J. Synchrotron Rad.* **7**, 229–235.
Gallois, B., Real, J. A., Hauw, C. & Zarembowitch, J. (1990). *Inorg. Chem.* **29**, 1152–1158.
Guionneau, P., Marchivie, M., Bravic, G., Létard, J.-F. & Chasseau, D. (2004). *Topics in Current Chemistry*, Vol. 234, p. 97. Berlin: Springer-Verlag.
Gütlich, P. & Goodwin, H. A. (2004). Editors. *Topics in Current Chemistry*, Vol. 233, 234, 235. Berlin: Springer-Verlag.
Gütlich, P., Hauser, A. & Spiering, H. (1994). *Angew. Chem. Int. Ed. Engl.* **33**, 2024–2054.
Hansen, N. K., Fertey, P. & Guillot, R. (2004). *Acta Cryst.* A**60**, 465–471.
Hauser, A. (1992). *Chem. Phys. Lett.* **192**, 65–70.
Herber, R. & Casson, L. M. (1986). *Inorg. Chem.* **25**, 847–852.
Honda, K., Naknishi, F. & Feeder, N. (1999). *J. Am. Chem. Soc.* **121**, 8246–8250.
Huby, N., Guérin, L., Collet, E., Toupet, L., Ameline, J.-C., Cailleau, H., Roisnel, T., Tayagaki, T. & Tanaka, K. (2004). *Phys. Rev. B*, **69**, 020101.
Hummel, W., Hauser, J. & Bürgi, H. B. (1990). *J. Mol. Graph.* **8**, 214–220.
Hundt, R., Schön, J. C. & Jansen, M. (2006). *J. Appl. Cryst.* **39**, 6–16.
Ichiyanagi, K., Hebert, H., Toupet, L., Cailleau, H., Guionneau, P., Létard, J.-F. & Collet, E. (2006). *Phys. Rev. B*, **73**, 060408.
Johnson, C. K. (1976). *ORTEPII*. Report ORNL-5738, Oak Ridge National Laboratory, Oak Ridge TN, USA.
Katrusiak, A. & McMillan, P. F. (2004). *Crystallography at High Pressure*, edited by A. Katrusiak & P. F. McMillan, *NATO Science Series II: Mathematics, Physics and Chemistry*. Dordrecht: Kluwer Academic Publishers.
König, E. & Madeja, K. (1967). *Inorg. Chem.* **6**, 48–55.
Kovalevsky, A. Y., King, G., Bagley, K. A. & Coppens, P. (2005). *Chem. Eur. J.* **11**, 7254–7264.
Kusz, J., Schollmeyer, D., Spiering, H. & Gütlich, P. (2005). *J. Appl. Cryst.* **38**, 528–536.
Kusz, J., Spiering, H. & Gütlich, P. (2000). *J. Appl. Cryst.* **33**, 201–205.
Kusz, J., Spiering, H. & Gütlich, P. (2001). *J. Appl. Cryst.* **34**, 229–238.
Lee, J. J., Sheu, H. S., Lee, C. R., Chen., J. M., Lee, J. F., Wang, C. C., Huang, C. H. & Wang, Y. (2000). *J. Am. Chem. Soc.* **122**, 5742–5747.
Legrand, V. (2005). PhD thesis, University Henri Poincaré – Nancy 1, No. 1132.
Legrand, V., Pillet, S., Carbonera, C., Souhassou, M., Létard, J.-F., Guionneau, P. & Lecomte, C. (2007). To be published.
Legrand, V., Pillet, S., Souhassou, M., Lugan, N. & Lecomte, C. (2006). *J. Am. Chem. Soc.* **128**, 13921–13931.
MacLean, E. J., McGrath, C. M., O'Connor, C. J., Sangregorio, C., Seddon, J. M. W., Sinn, E., Sowrey, F. E., Teat, S. J., Terry, A. E., Vaughan, G. B. M. & Young, N. A. (2003). *Chem. Eur. J.* **921**, 5314–5322.
Marchivie, M., Guionneau, P., Howard, J. A. K., Chastanet, G., Létard, J. F., Goeta, A. E. & Chasseau, D. (2002). *J. Am. Chem. Soc.* **124**, 194–195.
Marchivie, M., Guionneau, P., Létard, J. F., Chasseau, D. & Howard, J. A. K. (2004). *J. Phys. Chem. Solids*, **65**, 17–23.
Money, V. A., Radosavljevic Evans, I., Halcrow, M. A., Goeta, A. E. & Howard, J. A. K. (2003). *Chem. Commun.* pp. 158–159.
Niel, V., Thompson, A. L., Goeta, A. E., Enachescu, C., Hauser, A., Galet, A., Muñoz, M. C. & Real, J. A. (2005). *Chem. Eur. J.* **11**, 2047–2060.
Ohba, S. & Ito, Y. (2003). *Acta Cryst.* B**59**, 149–155.
Oxford Diffraction (2004). *CrysAlis CCD* and *CrysAlis RED*. Versions 1.171. Oxford Diffraction, Wrocław, Poland.
Ozawa, Y., Pressprich, M. R. & Coppens, P. (1998). *J. Appl. Cryst.* **31**, 128–135.
Paciorek, W. A., Meyer, M. & Chapuis, G. (1999). *Acta Cryst.* A**55**, 543–557.
Pillet, S., Hubsch, J. & Lecomte, C. (2004). *Eur. Phys. J. B*, **38**, 541–552.
Pillet, S., Legrand, V., Souhassou, M. & Lecomte, C. (2006). *Phys. Rev. B*, **74**, 140101.
Pressprich, M. R., White, M. A. & Coppens, P. (1993). *J. Am. Chem. Soc.* **115**, 6444–6445.
Rajagopal, S., Schmidt, M., Anderson, S., Ihee, H. & Moffat, K. (2004). *Acta Cryst.* D**60**, 860–871.
Ribbe, P. H., Megaw, H. D., Taylor, W. H., Ferguson, R. B. & Traill, R. J. (1969). *Acta Cryst.* B**25**, 1503–1518.
Sheldrick, G. M. (1997). *SHELX97*. University of Göttingen, Germany.
Spiering, H., Meissner, E., Köppen, H., Müller, E. W. & Gütlich, P. (1982). *Chem. Phys.* **68**, 65–71.
Techert, S. & Zachariasse, K. A. (2004). *J. Am. Chem. Soc.* **126**, 5593–5600.
Thompson, A. L., Goeta, A. E., Real, J. A., Galet, A. & Muñoz, M. C. (2004). *Chem. Commun.* pp. 1390–1391.
Turowska-Tyrk, I. (2003). *Acta Cryst.* B**59**, 670–675.
Varret, F., Boukheddaden, K., Codjovi, E., Enachescu, C. & Linarès, J. (2004). *Topics in Current Chemistry*, Vol. 233, pp. 199–229. Berlin: Springer-Verlag.
Vorontsov, I. I. & Coppens, P. (2005). *J. Synchotron Rad.* **12**, 488–493.
White, M. A., Pressprich, M. R., Coppens, P. & Coppens, D. D. (1994). *J. Appl. Cryst.* **27**, 727–732.
Wulff, M., Schotte, F., Naylor, G., Bourgeois, D., Moffat, K. & Mourou, G. (1997). *Nucl. Instrum. Methods A*, **398**, 69–84.